

signed informed consent forms. All of them were informed about the purpose of the experiment, were able to discontinue participation at any time and no payment was provided for the participation. All subjects were blindfolded and instructed to move accordingly to the haptic feedback, but no instructions were given about their velocities. Since the surrounding sounds can probably modify the users' behavior as they could be afraid to hit something, we cut off the auditory feedback by reproducing white noise through earphones. Two different trajectories were considered for the robot in each modality (see Fig. 1.9). The clockwise and counterclockwise trajectories were about 225 m and 223 m long, respectively. Each one was composed by four clear long corridors (the width of the corridors ranged from 1.2 to 2.2 m) and eight 90 deg turns. Each subject performed 4 trials: 2 trials for each trajectory in a randomized order, thus the total number of considered trials was 60. In order to evaluate the proposed haptic policy, the subjects additionally performed 2 trials for each trajectory without any vision impairment. In this case the desired trajectory of the user was displayed by the laptop positioned on the mobile robot. It is worth noting that the experiments with blindfolded people were performed to show the validity of the proposed approach in the challenging scenario in which visual and also auditory information were not available. In other terms, blind-folding was meant more to prove how performant was our method more than specifically investigating guidance for blinds.

The robot had a map of the environment and autonomously localized itself via the Monte Carlo Localization [64] provided by the Aria Core Library [36]. The initial obstacle-free paths for both the robot and the user were computed offline using the RRT (Rapidly-exploring Random Tree) motion planner [34]. In addition, we considered 3 static virtual obstacles and 2 dynamic ones (see Fig. 1.9(a)-(b)). The obstacles were unknown to the robot, i.e, the initial paths did not consider such obstacles. We simulated a sensing range of 4 m for the robot. As soon as the obstacles were inside the sensing range of the robot, the actual path was updated online by running a new instance of the RRT planner. The camera was rotated about its x -axis of 23.20 deg. Regarding the formation parameters, we set $l^d = 1.1$ m and $\psi^d = \pi$, $k_1 = k_2 = 3$, $d = 0.1$ m, $\alpha = 0.8$ rad/s and $\delta = l^d - 0.2$ m. The parameters above were determined by both the mechanical limitations of the system and the environment, in order to allow the user to properly navigate and accomplish the goal.

For each trajectory we computed the formation error $\mathbf{E}(t) = \mathbf{P}_h(t) - \mathbf{P}_r(t) - l^d (\cos \psi^d, \sin \psi^d)^T$. Figs. 1.10-1.11 show the trials in which lowest formation error was achieved. In Fig. 1.10(a), Fig. 1.11(a) is reported the actual position of the reference point $\mathbf{P}_h(t)$ and its desired pose computed as $\mathbf{P}_r(t) + l^d (\cos \psi^d, \sin \psi^d)^T$. Fig. 1.10(b) and Fig. 1.11(b) show the time evolution of the norm of the formation error $\mathbf{E}(t)$ for both trajectories. Peaks in the formation error are mainly due to the rotational velocity of the robot in correspondence of sharp turns and to inaccurate estimations of the human's pose. The related vibrational frequencies of the haptic devices are reported in Fig. 1.10(c) and Fig. 1.11(c).

Figs. 1.12(a), 1.13(a) show the formation error for each trial $\mathbf{E}^i(t)$, $i = 1, 2, \dots, 60$. The percentage of time with respect to the total duration of the trial in which the vibrotactile bracelet was activated is reported in Figs. 1.12(b), 1.13(b). Finally in Figs. 1.12(c), 1.13(c) is reported the mean (and the standard deviation) of the linear velocity of the users for each trial $v_h^i(t)$, $i = 1, 2, \dots, 60$. In blue are reported the subjects who participated in the evaluation of the haptic devices (cf. Sec. 1.2.8). As we can notice, for both trajectories the mean of the formation error is always smaller than 0.3 m. Moreover, users who never tried the haptic wristband before were able to correctly recognize the haptic stimuli and follow the robot.

Results show the functionality of the proposed approach. For the clockwise and counterclockwise trajectories, the mean of the formation error $\mathbf{E}^i(t)$ among all the trials is 0.24 ± 0.04 m and 0.23 ± 0.05 m, the average percentage of time in which the bracelets are turned on is 26.65 ± 7.10 % and 24.41 ± 6.91 %, the average of the users' linear velocities is 0.62 ± 0.07 m/s and 0.63 ± 0.08 m/s. Concerning the activation time of the bracelets it is worth noting that also during a straight line, the bracelets may correct the trajectory of the users due to the well known fact that it is hard for a blindfolded people to walk exactly straight due to the absence of landmarks. Thus, also a straight line can reveal if the proposed approach is valid and the bracelet can thus be activated during such a path. For the linear velocities of the subjects, it is worth noting that we asked the subjects to walk at their comfortable speed. Moreover, due to the reduced activation of the *slow down* behavior,

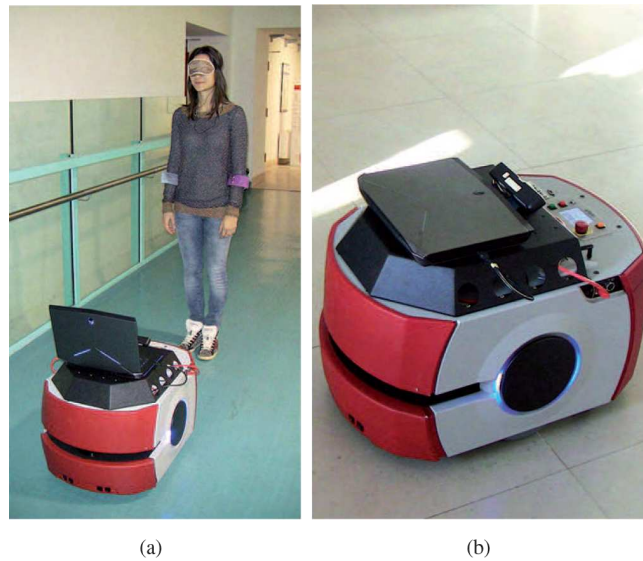


Figure 1.8: Experimental setup: the human subject is blindfolded and instructed to move accordingly to the haptic feedback provided by two custom-design vibrotactile bracelets. (b) Pioneer LX robot equipped with a backward facing Asus Xtion camera.

the users' linear velocities are mainly determined by the confidence of the users in the system.

Experiments performed on users with no vision impairments reveal that for the clockwise and counterclockwise trajectories the formation error $E^i(t)$ among all the trials is 0.15 ± 0.03 m and 0.13 ± 0.02 m, and the average of the users' linear velocities is 0.82 ± 0.08 m/s and 0.79 ± 0.07 m/s.

1.2.13 Results and Discussion

Although these results are promising, a comparison between the results obtained using this approach and experiments performed with sighted people reveal that additional studies need to be done in order to have comparable formation errors and walking speeds.

The proposed haptic feedback policy assumes that users behave like unicycle systems and smoothly rotate when a proper vibrotactile stimulus is received. Under these assumptions, the haptic feedback can direct the user toward the desired pose until she/he is close enough to it. If the user sharply turns when a stimulus is received, it becomes harder for the proposed method to correctly guide her/him, mainly due to delays in the reaction time of the user. However, this situation never happened in our experimental validation.

We designed the system in a way that the user always remains in charge of the final decision to take and she/he can always override the "suggestions" given by the system. A possible drawback of such a decision is that, in case of danger, the proposed system can not force the user to move in a particular way. This problem is indeed shared among all approaches that use tactile feedback.

The Asus Xtion offers a 58 deg horizontal wide viewing angle and an effective sensing range of 0.8-3.5 m. It works well in an almost completely open environment, however its real world uses can be limited. In the proposed experiments we showed that it is possible to use such a sensor also in less open environments: the human was correctly tracked around a series of 90 deg turns through hallways by using a proper choice of formation parameters and trajectory for the robot. It is worth noting that the formation parameters (l^d, ψ^d) should be accurately tailored depending on the sensors' characteristics and on the environment. For example, big values of l^d will make the system not usable in less open environments since the user may collide with the walls during sharp turns.

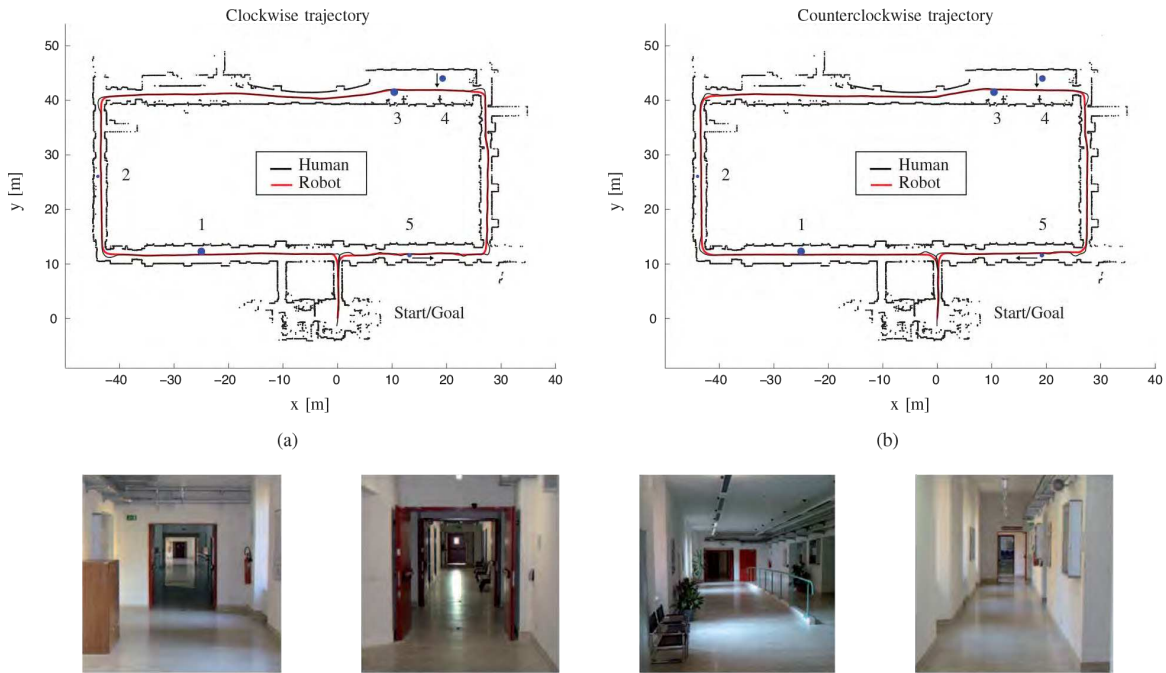


Figure 1.9: *Experimental scenario.* The experimental scenarios contain a goal region and virtual dynamic and static obstacles (blue). The objective is to guide the user from her/his starting position to the goal one while avoiding obstacles. We consider three static obstacles (obstacles 1, 2, and 3) and two moving obstacles (obstacles 4 and 5). The black arrows represent the velocity directions of the dynamic obstacles. The speed of the moving obstacles is 0.4 and 0.5 m/s, respectively for obstacle 4 and 5. Each user performed the proposed trajectory four times: two times in a clockwise order (a) and twice in a counterclockwise order (b). A Rapidly-exploring Random Tree was used to generate the initial trajectories for both the robot and the user. The initial trajectories do not consider the obstacles which are unknown to the users. For the obstacles, we considered a sensing range of 4 m for the robot, i.e, when an obstacle is inside the sensing range the Rapidly-exploring Random Tree is used to update the current trajectories. (c) Sample images of the environment.

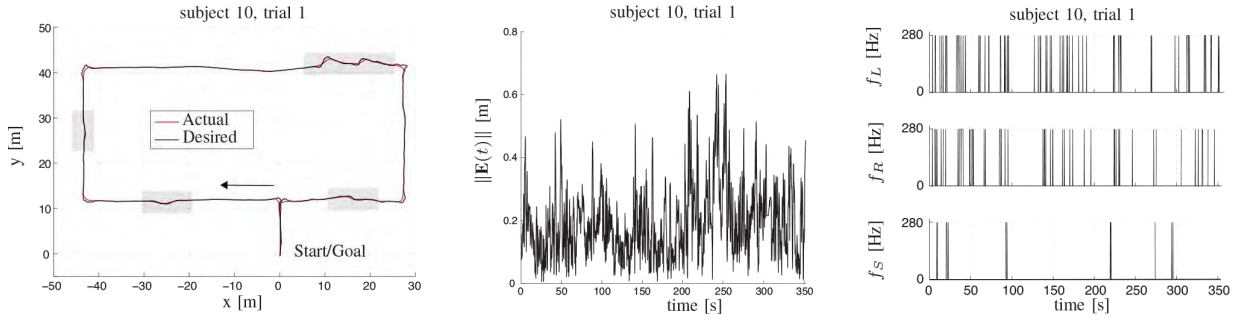


Figure 1.10: *Experimental results, clockwise trajectory.* (a) Desired and actual trajectories performed by the users, the shaded areas represent the portions of the trajectory which were update due to the presence of static and dynamic obstacles; (b) formation error $\mathbf{E}(t) = (E_x(t), E_y(t))^T$; (c) bracelets activation time for the users who achieved the lowest formation error.

12

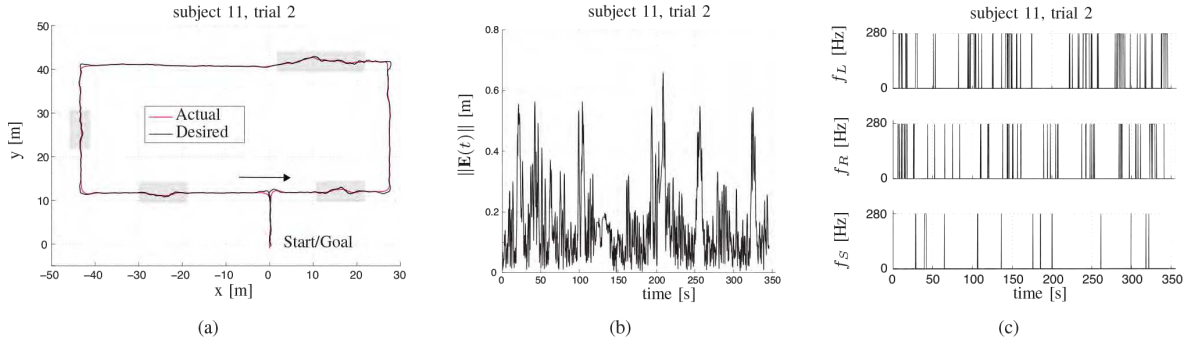


Figure 1.11: *Experimental results, counterclockwise trajectory.* (a) Desired and actual trajectories performed by the users, the shaded areas represent the portions of the trajectory which were update due to the presence of static and dynamic obstacles; (b) formation error $\mathbf{E}(t) = (E_x(t), E_y(t))^T$; (c) bracelets activation time for the users who achieved the lowest formation error.

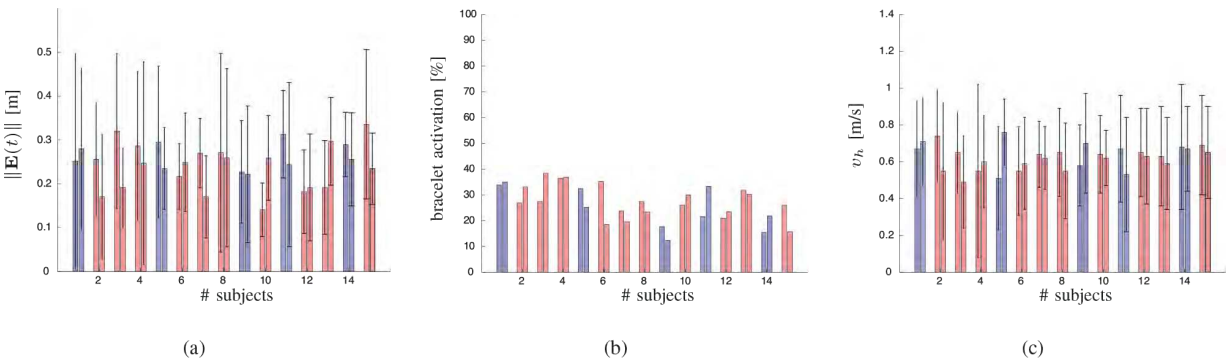


Figure 1.12: *Experimental results for the clockwise trajectory.* (a) Mean and standard deviation of the norm of the formation error $\mathbf{E}(t) = (E_x(t), E_y(t))^T$ over the 60 trials for the 15 subjects. (b) Percentage of activation time of the bracelets with respect to the trajectory execution time. (c) Mean and standard deviation of the linear velocity $v_h(t)$ of the users. In red are reported the subjects which did not participate in the evaluation of the haptic bracelet.

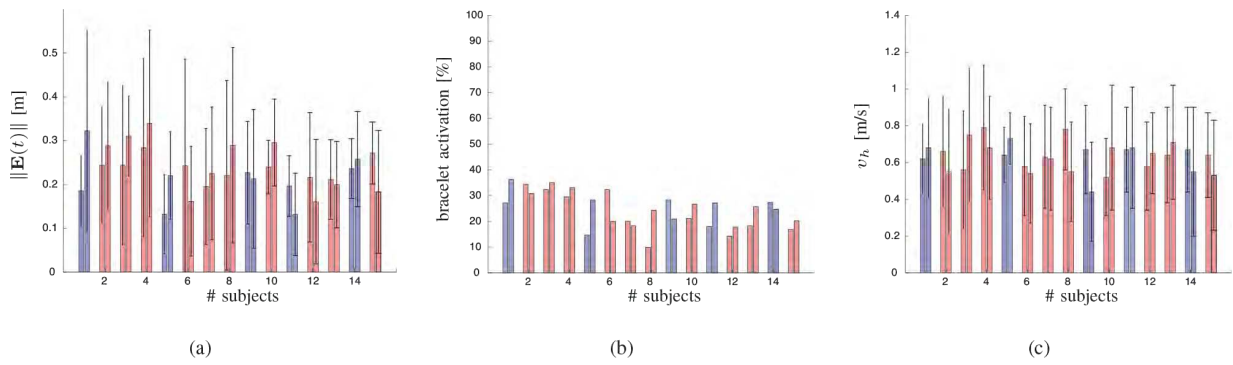


Figure 1.13: *Experimental results for the counterclockwise trajectory.* (a) Mean and standard deviation of the norm of the formation error $\mathbf{E}(t) = (E_x(t), E_y(t))^T$ over the 60 trials for the 15 subjects. (b) Percentage of activation time of the bracelets with respect to the trajectory execution time. (c) Mean and standard deviation of the linear velocity $v_h(t)$ of the users. In red are reported the subjects which did not participate in the evaluation of the haptic bracelet.

1.3 Path planner

The main source of inspiration for the predictive approach came from [18], where the authors developed a predictive haptic method based on a look-ahead algorithm. The algorithm was evaluated in virtual environment, where users were asked to steer a vehicle along a path by using a customized grounded haptic interface.

Let us consider a human $\mathbf{x}(t) = [x(t), y(t), \theta(t)]^T$ whose kinematics can be abstracted as a unicycle model (see Figure 1.14), where $[x(t), y(t)]^T$ and $\theta(t)$ represent the position and orientation of the human w.r.t. the world reference frame $\langle O_w, X_w, Y_w, Z_w \rangle$ at time $t \in \mathbb{R}_{>0}$, respectively. Let $v(t)$, $\omega(t)$ be the linear and angular velocities of the human, respectively. The human kinematics is described as

$$\dot{\mathbf{x}}(t) = \begin{bmatrix} \cos(\theta(t)) \\ \sin(\theta(t)) \\ 0 \end{bmatrix} v(t) + \begin{bmatrix} 0 \\ 0 \\ 1 \end{bmatrix} \omega(t). \quad (1.7)$$

Let us consider the problem of steering the human locomotion in order to guide the user along a predefined path. This problem is referred to as path following problem. Let us briefly recall a common solution to it, [12]. Referring to Figure 1.14, let \mathcal{P} be a path to be followed which is parameterized by its arc length, $[x_T, y_T]^T$ be the orthogonal projection of the human on the path, θ_T be the orientation of the tangent to the path at $[x_T, y_T]^T$ w.r.t. X_w (the x -axis of the Frenet-Serret frame at $[x_T, y_T]^T$), d be the signed distance between $[x, y]^T$ and $[x_T, y_T]^T$, and $\tilde{\theta} = \theta - \theta_T$ be the heading of the human with respect to the path. Let $s \in \mathbb{R}$ be the curvilinear coordinate along the path, and $c(s)$ the curvature at that point, defined as $c(s) = d\theta_T/ds$.

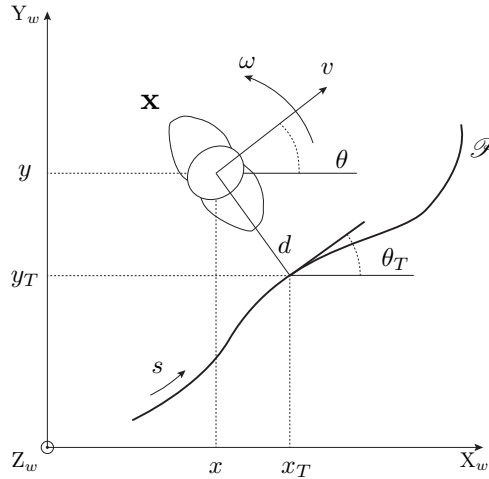


Figure 1.14: Path following setup: d represents the coordinate of the user position along the y -axis of the Frenet-Serret frame at $[x_T, y_T]^T$, i.e., the signed distance between the human and the orthogonal projection on to the path, θ_T and θ represent the angle between the x -axis of the world frame $\langle O_w, X_w, Y_w, Z_w \rangle$ and the x -axis of the Frenet-Serret and human frame, respectively.

The path \mathcal{P} is chosen such that the radius of any tangent circle at two or more points of the path which does not contain any point of the curve is lower-bounded by some positive real number r_{min} , i.e., $|c(s)| \leq 1/r_{min}$, $\forall s \in \mathbb{R}$.

With this parameterization, we can rewrite (1.13) as

$$\begin{aligned} \dot{s}(t) &= v(t) \cos(\tilde{\theta}(t))(1/(1 - c(s(t))d(t))) \\ \dot{d}(t) &= v(t) \sin(\tilde{\theta}(t)) \\ \dot{\tilde{\theta}}(t) &= \omega(t) - v(t) \cos(\tilde{\theta}(t))(1/(1 - c(s(t))d(t))). \end{aligned} \quad (1.8)$$

Given \mathcal{P} on the $X_w - Y_w$ plane, $v(t)$ bounded, $\dot{v}(t)$ bounded, the path following problem consists in finding a smooth feedback control law

$$\omega(t) = \omega_d(t) = k(s(t), d(t), \tilde{\theta}(t), v(t))$$

such that $\lim_{t \rightarrow \infty} d(t) = 0$ and $\lim_{t \rightarrow \infty} \tilde{\theta}(t) = 0$.

A linear feedback control law which stabilizes (1.8) is of the type

$$\omega_d(t) = -k_2 v(t) d(t) - k_3 |v(t)| \tilde{\theta}(t) + a(t)$$

where

$$a(t) = v \cos(\tilde{\theta}(t)) \frac{c(s(t))}{1 - c(s(t))d(t)},$$

is a corrective term coming from (1.8).

A nonlinear control approach for the same path following problem, holding asymptotic stability, is

$$\omega_d(t) = -k_2 d(t) v(t) \frac{\sin(\tilde{\theta}(t))}{\tilde{\theta}(t)} - k_3 |v(t)| \tilde{\theta}(t) + a(t), \quad (1.9)$$

being $k_2, k_3 \in \mathbb{R}_{>0}$, $v \neq 0$, and $\lim_{t \rightarrow \infty} v(t) \neq 0$.

1.3.1 Vibrotactile feedback and user response time

In order to properly steer the user, we provide vibrotactile stimuli via two haptic bracelets [55]. Such devices will be included in the FriWalk since its preliminary prototype. Each bracelet is made by two motors with a vibration frequency range of 100-280 Hz (the maximal sensitivity is achieved around 200-300 Hz, [52]), and typical normalized amplitude of 0.5 g. In order to not overload the tactile channel and to not reduce the recognition time, we do not modulate the frequency of the signal, but we use a simple on/off mechanism, similar to [54]. Thus, an attractive haptic feedback mechanism is adopted: vibration of the left bracelet alerts the participant to turn left, and vice versa. When a bracelet is engaged, its motors alternatively vibrate for 0.2 s at a frequency of 250 Hz.

Differently from [54], where a vibrotactile feedback was sent if the difference between the human angular velocity and the one computed from the controller was above a given threshold, here we set proper thresholds d_{th} , $\tilde{\theta}_{th} \in \mathbb{R}_{>0}$ on the position and orientation errors between the user and the path. Thus, if the absolute values of $d(t)$ and $\tilde{\theta}(t)$ are below the given thresholds, the angular velocity computed from the path following controller is zero. As a consequence, the proposed haptic feedback policy consists in sending a proper vibrotactile signal if the angular velocity $\omega_d(t)$ computed from the controller is not zero. In particular, the right bracelet is engaged if $\omega_d(t) < 0$, while the left bracelet is activated if $\omega_d(t) > 0$.

For evaluating the response time of the user to the vibrotactile stimuli, we tested the proposed haptic policy with seven healthy subjects (six males, age range 23-40, five right-handed). Participants were instructed to walk along a walkway, of about 4 m, whilst wearing the bracelets and to react accordingly to the stimulus type (turn left or turn right), as soon as they perceived it. The stimulus was sent as soon as the users have walked for 1 m. The bracelet continued to vibrate for 2 s after the activation. For each stimulus type, every subject performed 12 trials, organized in a pseudo-random order. All subjects were blindfolded and wore circumaural headphones, reproducing white noise to mask distracting ambient or cuing sounds from the bracelets. Human motion was tracked via an optical tracking system (Vicon Motion Systems Ltd, Oxford, UK).

The average time elapsed between the sending of the haptic stimulus and its actual perception by users, i.e., the start of their turning, was approximately 0.94 s, with a standard deviation of 0.23 s. This information about the delay is then used in the predictive approach, described in the following.

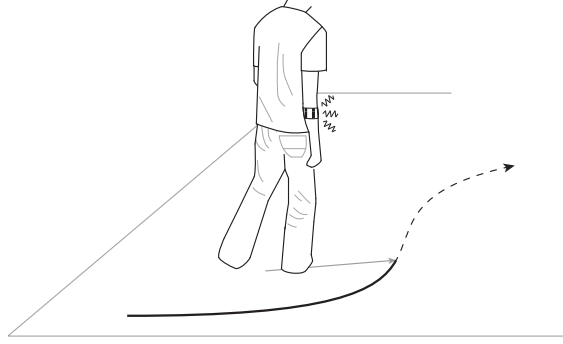


Figure 1.15: In the proposed scenario the human is steered along a predefined path via haptic signals provided by two vibrotactile bracelets.

1.3.2 A predictive approach for human guidance

An assumption of our approach is that the human responds to vibrotactile haptic stimuli with a certain delay. This means that the actuation of the angular input $\omega(t)$ in (1.13) is in fact delayed, i.e., $\omega(t - \delta)$, being $\delta \in \mathbb{R}_{>0}$ the response delay to the guiding stimulus.

Our purpose is to compute a proper control input $\omega_d(t)$, which will guide the user along the path when she/he will actuate it at time $t + \delta$. By considering the angular velocity actuation as $\omega(t - \delta)$ and by shifting the system (1.13) of δ , we can rewrite the path following control in (1.9) as

$$\omega_d(t) = -k_2 d(t + \delta) v(t + \delta) \frac{\sin(\tilde{\theta}(t + \delta))}{\tilde{\theta}(t + \delta)} - k_3 |v(t + \delta)| \tilde{\theta}(t + \delta) + a(t + \delta).$$

Thus, we need to compute a prediction of the user at time $t + \delta$ in order to compute the correct control input $\omega_d(t)$.

Due to the intrinsic discrete functioning of the computation machines, in what follows we switch from continuous time $t \in \mathbb{R}_{>0}$ to discrete time $k \in \mathbb{N}$. This means that we consider the actuation delay $\delta \in \mathbb{R}_{>0}$ as $\Delta \in \mathbb{N}$, which is a multiple of time step, and that we compute a desired angular velocity $\omega_{d,k}$, Δ steps in the future.

1.3.3 Human tracking at time k

Optical tracking systems are widely used for human tracking in indoor environment. Even though these systems bring high precision and accuracy on the measurements, the acquired data are in general limited to the human position and orientation in space. In our approach, we have the necessity of a complete human state, i.e., human position, orientation, linear, and angular velocity, thus measurements from optical tracking systems are not enough. For obtaining such state, we exploited an Extended Kalman Filter (EKF) algorithm [40], so that we could use a reliable estimate of the human linear and angular velocities, together with its position and orientation. Let us consider a non-linear system, with the following dynamics

$$\begin{aligned} \mathbf{X}_{k+1} &= f_k(\mathbf{X}_k) + w_k \\ \mathbf{Y}_k &= h_k(\mathbf{X}_k) + v_k \end{aligned}$$

where $\mathbf{X}_k \in \mathbb{R}^n$ is the state of the system, \mathbf{Y}_k are sensor measurements, $f_k(\mathbf{X}_k) : \mathbb{R}^n \rightarrow \mathbb{R}^n$ is the state update, $h_k(\mathbf{X}_k) : \mathbb{R}^n \rightarrow \mathbb{R}^m$ are measurements reading at step k , and $v_k \in \mathbb{R}^m$, $w_k \in \mathbb{R}^n$ are white Gaussian,

independent processes with zero mean and covariance matrices $E[v_k v_k^T] = R_k$ and $E[w_k w_k^T] = Q_k$. The initial system condition \mathbf{X}_0 is considered as a Gaussian random vector, i.e., $\mathbf{X}_0 \sim \mathcal{N}(\bar{\mathbf{X}}_0, P_0)$.

The EKF algorithm used for the our predictive approach is

$$\begin{aligned}\hat{\mathbf{X}}_{k+1}^- &= f_k(\hat{\mathbf{X}}_k^+), \\ P_{k+1}^- &= F_k P_k^+ F_k^T + Q_k,\end{aligned}\quad (1.10)$$

being

$$\begin{aligned}K_{k+1} &= P_{k+1}^- H_{k+1}^T (H_{k+1} P_{k+1}^- H_{k+1}^T + R_{k+1})^{-1}, \\ \hat{\mathbf{X}}_{k+1}^+ &= \hat{\mathbf{X}}_{k+1}^- + K_{k+1} (\mathbf{Y}_{k+1} - h_{k+1} \hat{\mathbf{X}}_{k+1}^-), \\ P_{k+1}^+ &= (I - K_{k+1} H_{k+1}) P_{k+1}^-, \end{aligned}\quad (1.11)$$

and

$$F_k = (\nabla f)(\hat{\mathbf{X}}_k^+), \quad H_k = (\nabla h)(\hat{\mathbf{X}}_{k+1}^-),$$

being the Jacobian matrices of $f(\cdot)$ and $h(\cdot)$, i.e, the linearization of the system dynamics and of the observation dynamics around \mathbf{X}_k^+ and \mathbf{X}_{k+1}^- , respectively.

In our approach, the system state \mathbf{X}_k is defined as $\mathbf{X}_k = [\mathbf{x}_k^T, v_k, \omega_k]^T$, whereas the state evolution is based on the Euler integration method

$$f_k(\mathbf{X}_{k+1}) = \begin{bmatrix} x_{k+1} \\ y_{k+1} \\ \theta_{k+1} \\ v_{k+1} \\ \omega_{k+1} \end{bmatrix} = \begin{bmatrix} x_k + v_k \cos(\theta_k) \Delta t \\ y_k + v_k \sin(\theta_k) \Delta t \\ \theta_k + \omega_k \Delta t \\ v_k \\ \omega_k \end{bmatrix},$$

being $\Delta t = 1/f_V$ the discrete time step of the evolution of our system, and f_V the sampling rate of the measurements acquisition system. Since the process noise w_k is applied to the whole state, the human linear and angular velocity are modeled as “random walks”.

The Jacobian matrix F_k obtained by differentiating (1.13) w.r.t. to the state \mathbf{X}_k has the form

$$F_k = \begin{bmatrix} 1 & 0 & -v_k \sin(\theta_k) \Delta t & v_k \cos(\theta_k) \Delta t & 0 \\ 0 & 1 & v_k \cos(\theta_k) \Delta t & v_k \sin(\theta_k) \Delta t & 0 \\ 0 & 0 & 1 & 0 & \Delta t \\ 0 & 0 & 0 & 1 & 0 \\ 0 & 0 & 0 & 0 & 1 \end{bmatrix},$$

while H_k is set to be constant and equal to

$$H = \begin{bmatrix} 1 & 0 & 0 & 0 & 0 \\ 0 & 1 & 0 & 0 & 0 \\ 0 & 0 & 1 & 0 & 0 \end{bmatrix}.$$

The covariance matrices were chosen constant and not dependent on k , i.e., $R_k = R_0$ and $Q_k = Q_0$.

1.3.4 Human prediction at time $k + \Delta$

Since the actuation delay introduced by the human is Δ , we want to predict the human state Δ steps ahead from its current estimate at step k , i.e., $\mathbf{X}_{k+\Delta}^- = f_k^p(\mathbf{X}_k^+)$. For doing this, we consider a prediction step of the form

$$f_k^p(\mathbf{X}_k^+) = \begin{bmatrix} x_k + r_k \sin(\theta_{k+\Delta}) - r_k \sin(\theta_k) \\ y_k - r_k \cos(\theta_{k+\Delta}) + r_k \cos(\theta_k) \\ \theta_k + \omega_k \Delta \\ v_k \\ \omega_k \end{bmatrix}, \quad (1.12)$$

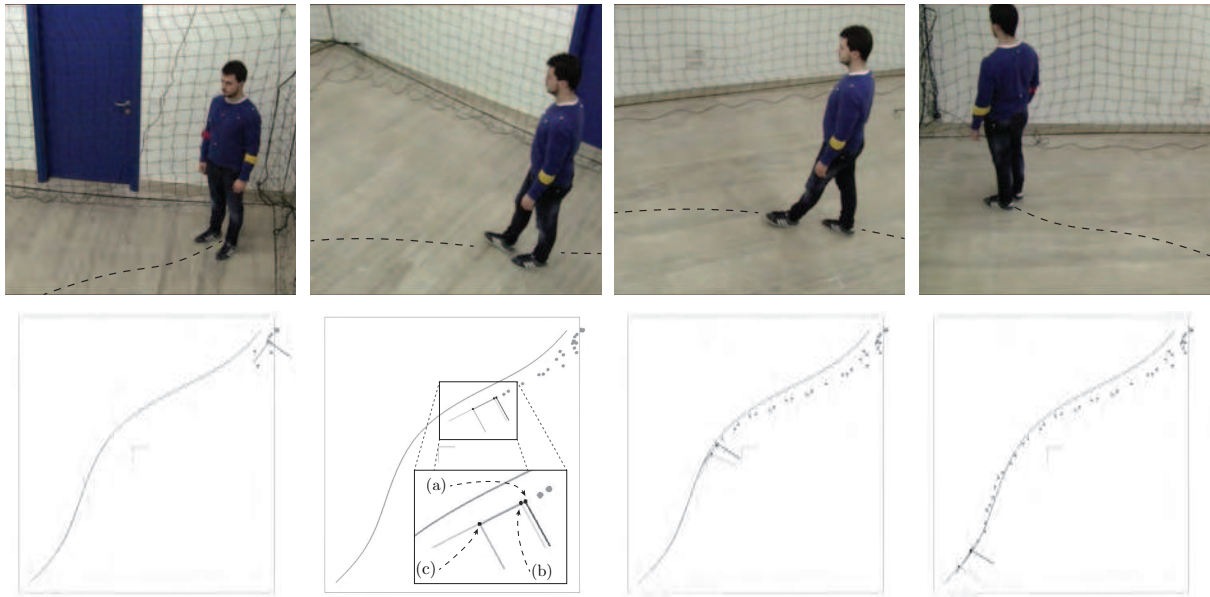


Figure 1.16: Particular of a trial, VP modality: the subject is equipped with two vibrotactile bracelets, one per arm, and with eight passive retroreflective optical markers (visible in the upper row). The user is asked to walk at his natural walking speed following the haptic stimuli sent by the system. The subject is able to see the environment, but has no visual cue about the path (depicted for the reader in the upper figures). In the inset, the human actual position (a), the EKF filtered state (b), and the predicted state (c) are shown.

being $r_k = v_k/\omega_k$ the radius of the arc of circle routed by the human at step $k + \Delta$, and considering v_k and ω_k constant between k and $k + \Delta$.

In our predicting approach, we consider ω_k constant even if during Δ steps some angular velocity controls could be applied by the guidance system, resulting in changes in the actual value of ω_k . However, at this stage of the development, we preferred to not model the variation of the angular velocity of the user when a haptic stimuli is perceived. In fact, from our evaluation on the activation delay (see Sect. 1.3.1), we estimated a mean value for the amount of angular velocity variation applied by the human, together with its standard deviation. However, due to its high variability, we decided to not consider it. As a consequence, we modeled the linear and angular velocity evolution as a “random walk”.

1.3.5 Experimental Validation

We here present its evaluation of an approach for steering a human along a path by using haptic stimuli. We tested four conditions:

- VN: the subject had no vision impairment (V), and the human state prediction Δ steps in the future was not enabled (N);
- BN: the subject was blindfolded (B), and the human state prediction Δ steps in the future was not enabled (N);
- VP: the subject had no vision impairment (V), and the human state prediction Δ steps in the future was enabled (P), using (1.12) for obtaining the control law $\omega_{d,k}$;
- BP: the subject was blindfolded (B), and the human state prediction Δ steps in the future was enabled (P), using (1.12) for obtaining the control law $\omega_{d,k}$;

In all modalities, participants were asked to walk along a pathway while directional cues concerning an ideal path to follow were sent to them in form of haptic stimuli (see Figure 1.16). We tested our guidance system also with a blindfolded modality for having visibility situations similar to those frequently encountered in search and rescue scenarios. Participants were equipped with two vibrotactile bracelets, one per arm, and were allowed to choose their natural walking speed in order to perform the task. The human was modeled as a unicycle robot, and its state \mathbf{X}_k was tracked with an EKF (1.10)-(1.11). Measurements \mathbf{Y}_k corresponding to human poses were acquired with an optical tracking system (Vicon Motion Systems Ltd, Oxford, UK), composed of eight cameras. Participants wore eight passive retroreflective optical markers located on their torso, since there is a strong analogy between the steering wheels of a mobile robot and the human trunk [3]. The sampling frequency of the motion capture system was set to $f_V = 100$ Hz. The four modalities were tested on five different paths (see Figure 1.17, both columns): one linear path (first row), one path with low curvature (second row), one path with high curvature (fourth row), and their flipped versions (third and fifth rows).

The evaluation was performed on seven healthy subjects (five males, age range 19-65, four right-handed): two of them had great experience with the proposed vibrotactile bracelets; the remaining users had no experience with the vibrotactile interfaces. Two of them participated in the evaluation of the actuation delay (see Sect. 1.3.1). None of the participants reported any deficiencies in perception abilities or physical impairments. The participants signed informed consent forms. All of them volunteered to the experiment, were informed about the purpose of the it, and were able to discontinue participation at any time. The trials were arranged in a pseudo-random order, whose list was the same for all the participants. Each participant performed 40 trials, i.e., four modalities repeated two times for each path, thus resulting in 280 collected trials (70 trials per modality).

For what regards the evaluation parameters, the distance and the orientation thresholds were chosen as $d_{th} = 0.15$ m and $\theta_{th} = 0.26$ rad = 15 deg, respectively. The distance and orientation thresholds were chosen so that they would take in account natural oscillations of the human locomotion. The optical motion tracking frame rate f_V was set to 100 Hz, and the path following control for $\omega_{d,k}$ was computed every 20 steps (equivalent to 0.2 s), according to the duration of the vibrotactile stimuli (see Sect. 1.3.1). Concerning the EKF parameters, we chose $\sigma_v = 0.05$, $\sigma_w = 0.05$, $P_0 = \mathbf{I}_5$, $R_0 = \text{diag}([0.01, 0.01, 0.03])$, and $Q_0 = \text{diag}([0.5, 0.5, 0.5, 0.5, 0.5])$, being \mathbf{I}_i an identity matrix of dimension i . The initial configuration for the EKF state $\tilde{\mathbf{X}}_0$ was chosen as the first point of the evaluated path (see Figure 1.17). The controller gains were chosen as $k_2 = 10$ and $k_3 = 15$. Finally, for what regards the human state prediction, the number of steps to look in the future was set to 100, i.e., $\Delta = 100$, which leads to have a prediction of 1 s in the future.

1.3.6 Results and Discussion

Figure 1.17 shows the ground truth paths and the trajectories performed by the users. Each row represents a different path. The first column reports the trajectories performed having the prediction of the human state disabled, while the second column depicts the trajectories performed using the predictive approach. For each trial j , the mean distance error from the path was computed as $e_j = \sum_{k=1}^N (||\tilde{\mathbf{x}}_k - \tilde{\mathbf{x}}_{k,T}||) / N$, being $\tilde{\mathbf{x}}_k = [x_k, y_k]^T$ the position of the human on the $X_w - Y_w$ plane at step k , $\tilde{\mathbf{x}}_{k,T} = [x_{k,T}, y_{k,T}]^T$ its closest Frenet-Serret frame center at step k , N the number of time steps the subject has taken to complete the trial, and $||\tilde{\mathbf{x}}_k - \tilde{\mathbf{x}}_{k,T}||$ the Euclidean norm between $\tilde{\mathbf{x}}_k$ and $\tilde{\mathbf{x}}_{k,T}$. For each modality, we computed the mean distance error $\bar{D} = \sum_{j=1}^{70} e_j / 70$. Similarly, we computed the mean linear velocity of the subject \bar{V} as the sum of the means of the linear velocities during each trial over the number of trials, and the mean haptic stimuli \bar{H} , which is the percentage of time subjects were stimulated with haptic interfaces over the duration of the trials. These results are summarized in Figure 1.18 and in Table 1.3.

Comparisons of means among visual impairments (modality V vs. modality B) and among state prediction (modality N vs. modality P) were tested using multiple repeated-measures ANalysis Of VAriance (ANOVA). In all conditions, collected data passed the Shapiro-Wilk normality test and the Mauchly's Test of Sphericity. A family-wise level $\alpha = 0.05$ has been used for all tests.

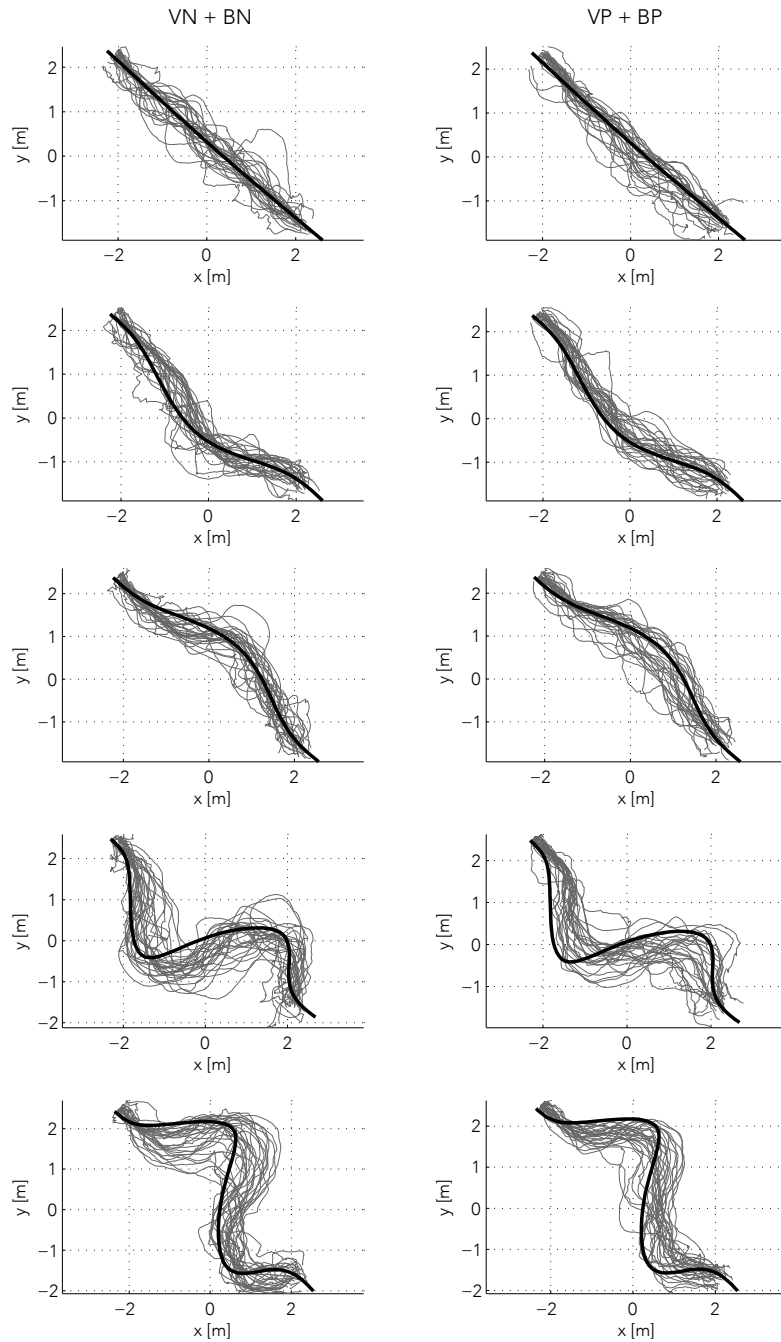


Figure 1.17: Predifined path and collected user trajectories. From top to bottom, both columns: linear path, low curvature path, flipped version of the low curvature path, high curvature path, flipped version of the high curvature path. Each path is depicted with a black line, while the trajectories performed by the subjects are shown with grey lines. The left column shows the trajectories performed by the participants during the non predicting modalities, i.e., VN and BN, while the right column shows the trajectories performed by the participants during the predicting modalities, i.e., VP and BP.

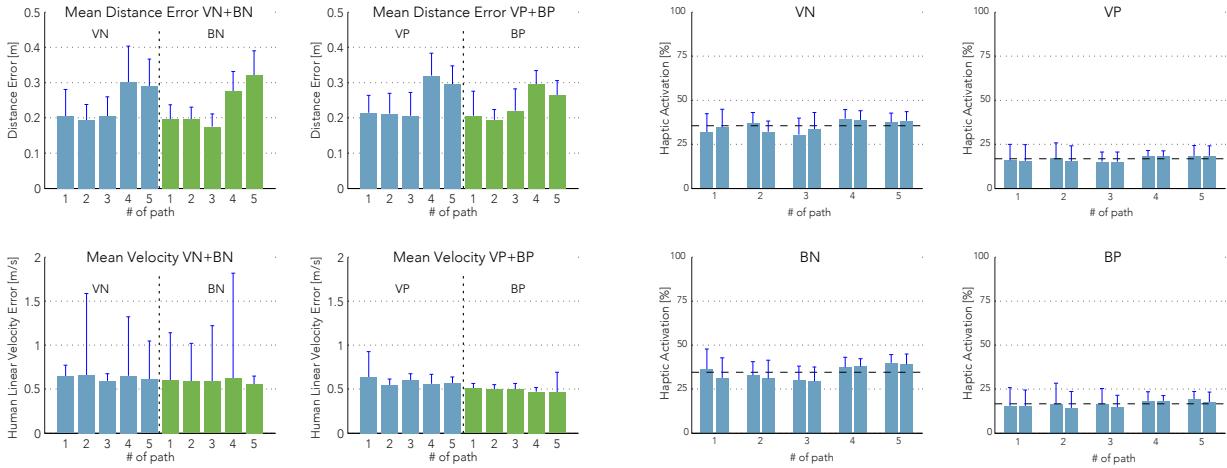


Figure 1.18: Mean error distance and mean human linear velocity for the given paths (a) and mean haptic activation (b) grouped by vision condition and by predicting modalities (columns). Each bar blue vertical lines depict the standard deviation from the mean value, whereas for (b) overall means among the collected data are marked with black dashed lines.

Modality	\bar{D} [m]	\bar{V} [m/s]	\bar{H} [%]
VN	0.24 (± 0.05)	0.63 (± 0.03)	35 (± 3.22)
BN	0.23 (± 0.06)	0.59 (± 0.02)	34 (± 3.97)
VP	0.25 (± 0.05)	0.58 (± 0.04)	17 (± 1.49)
BP	0.24 (± 0.04)	0.48 (± 0.02)	17 (± 1.67)

Table 1.3: Mean distance error \bar{D} , mean human linear velocity \bar{V} , and mean haptic stimuli activation \bar{H} (standard deviations are reported inside brackets).

From our results, we can say that the proposed predictive approach does not bring significant improvements to the path following problem for what concerns the distance error (see Figure 1.18(a), first row), which was in mean around 0.24 m. An analog consideration can be made for the human linear velocity (see Figure 1.18(a), second row), but in this case predicting the human state brought a significant reduction in the variability of the mean linear velocity itself, especially when the human was blindfolded, i.e., BN vs. BP modalities ($F(1, 4) = 68.23, p < 0.05$). For what regards the haptic activation time (see Figure 1.18(b)), the proposed predictive approach brought improvements, since the activation time of the bracelets is significantly lower when the predictive policy is used, VN vs. VP ($F(1, 4) = 974.00, p < 0.05$), and BN vs. BP modalities ($F(1, 4) = 277.93, p < 0.05$). Concerning the proposed haptic guidance, the obtained mean error of 0.24 m was deemed acceptable for the application at hand, considering also the distance and orientation thresholds, which were set as $d_{th} = 0.15$ m and $\theta_{th} = 15$ deg. From the performed evaluation, the proposed predictive approach did not improve the performance of the haptic guidance system in terms of distance error from the path. One of the possible motivations is that in the proposed algorithm we considered a fixed delay in the user response time. Moreover, in the prediction step, we did not model the variation of the angular velocity ω_k due to the perception of the haptic stimuli by the user. Checking whether a dynamic delay and/or a variation of the angular velocity ω_k as input can improve the performance in terms of distance error is in the scope of future works.

1.4 Obstacle Avoidance

As mentioned in the introduction of this document, let us focus on the problem of guiding users using the FriWalk toward a goal location in a dynamic environment while avoiding obstacle collisions. Possible scenarios are social activities suggested by the CPSN. Also in this policy, vibrotactile bracelets are used for guide the user in outdoor and indoor environments.

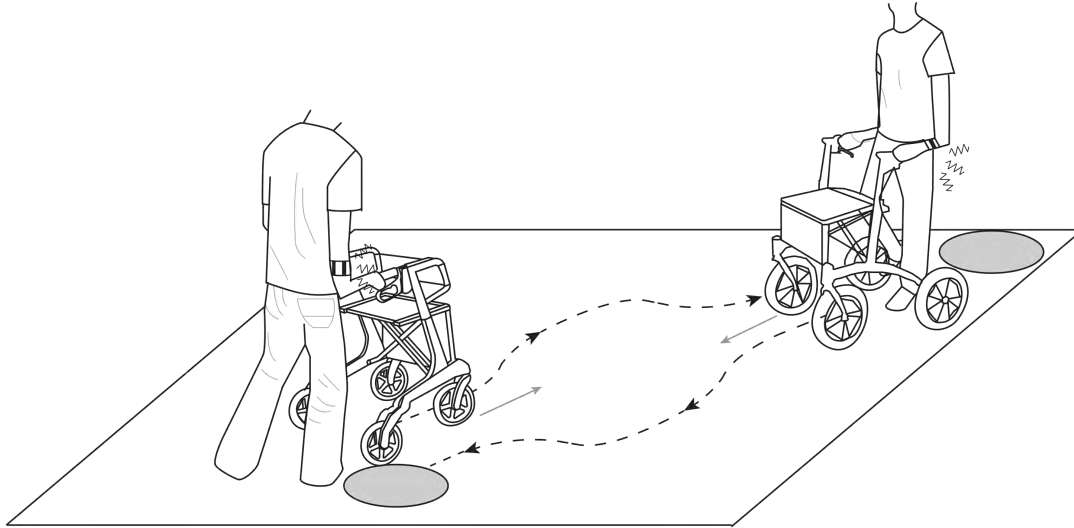


Figure 1.19: The subjects have to reach the respective goal areas while avoiding collisions with static obstacles (if present) and moving users. Each user wears two vibrotactile armbands which provide appropriate directional cues. A suitable obstacle avoidance policy is used to generate online haptic cues, which guide the users along collision-free trajectories (dashed).

1.4.1 Introduction

We developed a human guidance policy in order to guide multiple users along collision-free paths in dynamic environments by taking into account the user comfort in performing it. For each subject, the proposed method generates online suitable directional cues in order to minimize the possibility of collisions among the users. Directional cues are provided to the users via intuitive haptic stimuli displayed by two vibrotactile armbands. The users adjust their heading according to the perceived vibrations. The proposed method relies on Reciprocal Collision Avoidance for non-holonomic agents proposed in [2], that we adapt to our specific problem. It is worth pointing out that while it is simple to steer a robot, it is not trivial to impose a desired velocity to a human. The proposed human guidance algorithm takes into account the motion uncertainty of the users when reacting to a particular stimulus in order to minimize possible collisions among them and the environment.

We assume that the human locomotion can be approximated by the motion of a unicycle system, i.e., nonholonomic constraints similar to those of mobile robots seem to be at work when a human is walking [3]. This assumption allowed us to define an intuitive haptic policy which was successfully used to guide users also in mixed human-robot scenarios [58, 54, 56]. Moreover if the user is using the walker, the system (user plus cart) can be assimilated to an unicycle. In what follows, we assume that the human is free to select her/his desired walking speed. Control signals (i.e., haptic stimuli) are sent to the user in order to steer his locomotion. Requirements of our approach are that a person should always remain in charge of the final decision to take, the type of correction provided to the user should be perceived as very soft, and unnatural stimulations must be avoided as much as possible. Preliminary experiments were performed to evaluate the proposed guidance technique.

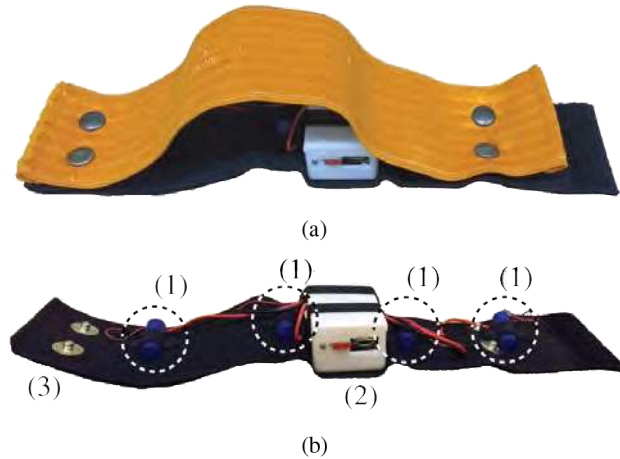


Figure 1.20: Directional cues are provided to the users via two vibrotactile armbands. The haptic armbands are composed of four vibrating motors (1) attached to an elastic band (3). A Li-Ion battery and a microcontroller are in (2). See 1.2.6 for further details.

1.4.2 Human guidance via haptic feedback

In this section, we briefly describe the human guidance algorithm. The proposed policy is based on the assumption that the human locomotion with or without the cart can be approximated by the motion of a unicycle system [3, 17]. Moreover, we assume that the human is free to select her/his desired walking speed. Thus, haptic stimuli are sent to the user in order to steer the heading. We modelled the pose of an user as aforementioned in 1.3. Thus the motion can be described as in 1.13,

$$\dot{\mathbf{x}} = \begin{bmatrix} \cos(\theta) \\ \sin(\theta) \\ 0 \end{bmatrix} v + \begin{bmatrix} 0 \\ 0 \\ 1 \end{bmatrix} \omega. \quad (1.13)$$

The problem of guiding a user towards a goal results in steering the human by acting on her/his angular velocity ω . Our purpose is to provide haptic stimuli in order to adjust the heading of the user.

In order to provide stimuli which are easily recognizable by the user, the device could elicit only three basic behaviors on the human (*turn left*, *turn right*, and *go straight*). Thus, only three stimuli would be sufficient in principle. As a consequence, we display vibrotactile stimuli via two haptic armbands placed on the forearms: vibration of the left armband alerts the participant to *turn left*, while vibration of the right armband alerts the participant to *turn right*. If the armbands do not vibrate, it means that the user can *go straight*. Each armband is an upgrade of the ones described in 1.2.6, as depicted in Figure 1.20.

1.4.3 Obstacle avoidance

In this section we describe the obstacle avoidance algorithm used to safely navigate the users in dynamic environments. In what follows, we assume that the agents (in our case the humans with or without the cart) are modeled as disc-shaped entities having radius r_i , $i = 1, \dots, n$, being n the number of agents. The algorithm is based on the extension of the Optimal Reciprocal Collision Avoidance (ORCA) [66], that we adapt to our specific problem.

The algorithm provides a sufficient condition for each agent to be collision-free for at least a fixed amount of time into the future. Each agent takes into account the observed velocity and pose of the other agents in order to avoid collisions with them. Then, the optimal velocity is selected by using linear programming.

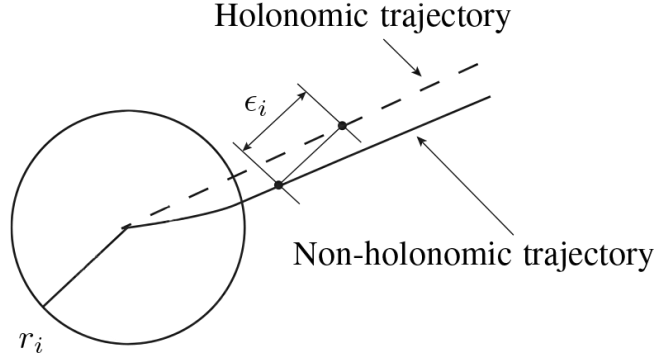


Figure 1.21: Every user is modeled as a disc-shaped entity having radius r_i , $i = 1, \dots, n$, being n the number of users. A non-holonomic agent i can track a holonomic speed vector with a certain tracking error ϵ_i . ϵ_i is used in the algorithm to compute the collision-free velocity.

Velocity-based collision avoidance approaches use the pose of the agents and their actual velocity to generate collision-free velocities [66, 67]. Guiding users via haptic, audio, or visual stimuli, implies that we are not imposing a desired velocity to the subjects (different from a robot). Instead, we provide stimuli which should be translated into suitable velocities. This arises two challenges. First, a mapping between the haptic stimuli and the velocity of the human should be defined. Second, motion uncertainty of the users when reacting to a given stimulus should be taken into account (cf. Sect. 1.4.1).

In order to define a relationship between the haptic stimuli and the velocity of the users, let us remind from Sect. 1.4.2 that we are interested in steering the users by changing their angular velocity ω (cf. Eq. (1.13)). Moreover, three stimuli (*turn left*, *turn right*, and *go straight*) have been demonstrated to be intuitive and effective in guiding users along path [1]. Thus, it is necessary to find the relationship between the proposed three stimuli and the angular velocity of the users. That is, we need to find the amount of angular velocity that the users apply when they perceive the proposed haptic stimuli.

For each user i , the algorithm calculates the holonomic velocities \mathbf{v}_i and related tracking errors ϵ_i from the following non-holonomic velocities (v_i, ω_{right}) , (v_i, ω_{left}) , $(v_i, 0)$, being $\omega_{right} = -1.11$ rad/s, $\omega_{left} = 1.08$ rad/s (cf. Table 1.4). The linear velocity v_i is estimated using an Extended Kalman Filter (cf. Sect. 1.4.4). Then, by using the holonomic velocities \mathbf{v}_i , constraints are added to the linear program in the ORCA formulation. Finally, the haptic stimuli related to the collision-free velocities are displayed to the users. It is worth pointing out that the collision-free velocities are computed in order to be as close as possible to the preferred ones. In our particular case, the preferred velocities are the ones that minimize the walking time of the users towards their goal areas.

From Table 1.4, we can observe that the users never *convert* a given haptic stimulus into the same exact angular velocity. Such motion uncertainty is taken into account by the obstacle avoidance method in the following way. Let $\omega = \mathcal{N}(\mu_\omega, \sigma_\omega)$ be a normal distribution of the actuated angular velocity (Table 1.4), and let $\mathbf{p}_i = \mathcal{N}(\mu_{\mathbf{p}_i}, \Sigma_{\mathbf{p}_i})$ be a bivariate normal distribution of the measured position \mathbf{p}_i of the user i , having mean $\mu_{\mathbf{p}_i}$ and standard deviation $\Sigma_{\mathbf{p}_i} = \text{diag}(\sigma_{\mathbf{p}_i}, \sigma_{\mathbf{p}_i})$.

Table 1.4: Mean and standard deviation of the angular velocity experimentally evaluated with 15 participants

Haptic stimulus	ω (rad/s)
<i>Turn left</i>	1.08 ± 0.31
<i>Turn right</i>	-1.11 ± 0.33
<i>Go straight</i>	0 ± 0.11

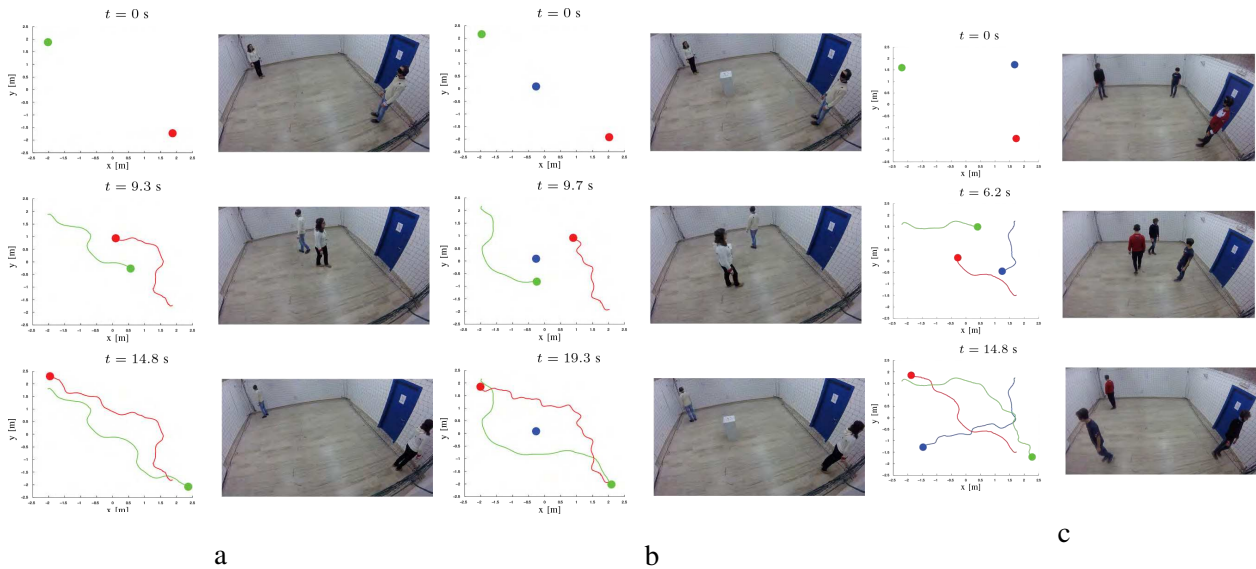


Figure 1.22: Experimental validation: (a) scenario S1. Two blindfolded and audio-occluded users have to move towards their goal areas by following directional cues provided by haptic armbands. The trajectories performed by the user are shown in red and green. (b) scenario S2. Two blindfolded and audio-occluded users have to move towards their goal areas, while avoiding a static obstacle. The trajectories performed by the user are shown in red and green, whereas the obstacle is depicted with a blue circle. (c) scenario S3. Three blindfolded and audio-occluded users are guided to reach the opposite corner of square room having side of 2 m. (Left) The trajectories performed by the user are shown in red, green, and blue. The users are represented with coloured circles. The starting point and the goal are two circles of radius 0.35 m centred in two opposite vertices of a square room with side of 2 m. (Right) Snapshots of a performed trial. Haptic stimuli are provided to the user via two vibrotactile wristbands.

1.4.4 Experimental Validation

We validated the proposed approach in three different scenarios. In the first scenario, two users were asked to reach two different goal areas, wearing two vibrotactile armbands (one per arm), which displayed the directional cues. We defined this scenario as S1. In the second scenario, S1 was augmented by introducing a static obstacle. Both users still had to reach two different goal areas, while avoiding the object. This scenario was named S2. The third scenario, named S3, was built by taking S1 and introducing a third human operator. A visual resume of the scenarios can be found in Figure 1.22. In all the three scenarios, the users tried two modalities. In a first modality (H), users were blindfolded and were wearing earphones for masking the distinguishable sounds of the vibro-tactile interfaces. In a second modality (V), users were able to see the environment and the other agents (other users or the obstacle), and no auditory occlusion was provided. In both modalities, users were allowed to choose their natural walking speed in order to perform the task. A Vicon optical tracking system, composed of eight cameras, was used to estimate the position of the user. The sampling frequency of the motion capture system was set to 100 Hz. In the experimental validation, we represented the users and the obstacles by their bounding circle; it is a common choice to represent objects by its bounding area or volume. The proposed evaluation was performed on 12 healthy subjects (all males, age range 23-49). None of the participants reported any deficiencies in perception abilities or physical impairments. The participants signed informed consent forms. All of them volunteered to the experiment, were informed about the purpose of the it, and were able to discontinue participation at any time. The motion control and related haptic stimulus was sent to the user each 0.2 s (5 Hz) according to the duration of the vibro-tactile stimuli (cf. Sect. 1.4.2-1.4.3).

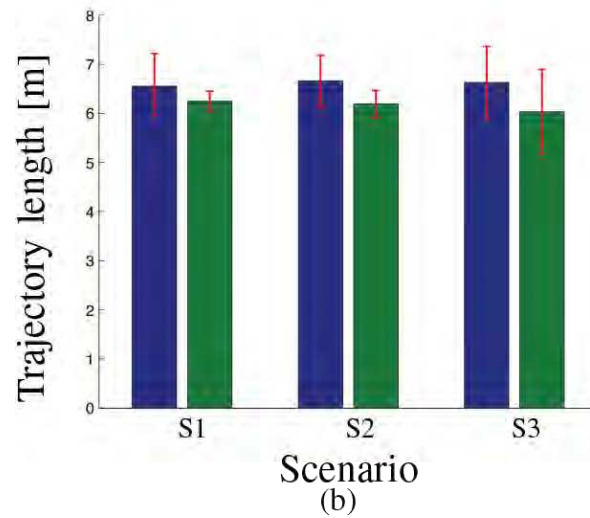


Figure 1.23: The length of the performed trajectories in the experimental validation, divided by scenario. Mean length of the path and standard deviation are reported. Blue bars represent data where haptics suggestions were provided to the users (H), whereas green bars represent data where visual information was provided to the users (V).

The participants performed four repetitions of scenario S1 and S2 per modality, being arranged in couples. For what concerns S3, triplets of users were formed. Four trials were performed per modality. In each trial, users were asked to start from a predefined positions and to reach a predefined goals. The users walked in a square room with a side of 2 m. The radius of the bounding circle was set to 0.35 m for each user. The starting point and the goal are two circles of radius 0.35 m. For the scenario S2, in which users were asked to avoid a static obstacle, we represented the obstacle with a 0.3 m circle. The goal was considered successfully reached as soon as the center of the bounding circle of the user entered the goal area.

Length of the trajectories was used as a metric to evaluate the algorithm. In all trials and for all the modalities, no collisions (with other agents either another user or the obstacle) happened. Whereas for the visual conditions this was expected, regarding the haptic guidance condition the obtained results show that our approach works. Figure 1.23 presents the recorded trajectory lengths for the three scenarios. In this case, the difference between visual trials (modality V) and situations where the users were suggested by haptic cues is not as vast as for the time to reach the goal.

1.4.5 Results and Discussion

With this work we addressed the problem of guiding multiple users with or without the FriWalk along collision-free paths exploiting haptic stimuli. The proposed navigation policy exploits the nonholonomic nature of human locomotion in goal directed paths, which leads to a very intuitive guidance mechanism. The proposed method is evaluated in three scenarios. Experimental results reveal that all the blindfolded subjects could safely reach the goal area. Although this result is promising, a comparison between the results obtained using this approach and experiments performed with sighted people reveals that additional studies need to be done in order to have comparable walking speed.

In future work, we plan to extend the proposed idea with the predictive approach presented in [1]. Finally, we will consider more challenging scenarios including the presence of narrow passages, and scenarios in which

the users have a limited interval of time to accomplish the task.

